Journal of Power Sources 568 (2023) 232831

Contents lists available at ScienceDirect

Journal of Power Sources

journal homepage: www.elsevier.com/locate/jpowsour

Experimental review of the performances of protective coatings for interconnects in solid oxide fuel cells

Mareddy Jayanth Reddy [a,*], Bartosz Kamecki [b,i], Belma Talic [c], Elisa Zanchi [d], Federico Smeacetto [d], John S. Hardy [e], Jung Pyung Choi [e], Łukasz Mazur [f], Robert Vaßen [g], Soumendra N. Basu [h], Tomasz Brylewski [f], Jan-Erik Svensson [a], Jan Froitzheim [a]

[a] Chalmers University of Technology, Department of Chemistry and Chemical Engineering, Kemivägen 10, 41296, Gothenburg, Sweden
[b] Advanced Materials Center, Faculty of Applied Physics and Mathematics, Gdańsk University of Technology, Gdańsk, 80-233, Poland
[c] Department of Sustainable Energy Technology, SINTEF Industry, Oslo, Norway
[d] Politecnico di Torino, Department of Applied Science and Technology – DISAT, Corso Duca degli Abruzzi 24, 10129, Torino, Italy
[e] Pacific Northwest National Laboratory, Battelle Memorial Institute, Electrochemical Materials and Devices Team, Energy and Environment Directorate, Richland, WA, United States
[f] AGH University of Science and Technology, Faculty of Materials Science and Ceramics, al. Mickiewicza 30, 30-059, Krakow, Poland
[g] Forschungszentrum Jülich GmbH, Institute of Energy and Climate Research, Materials Synthesis and Processing (IEK-1), 52425, Jülich, Germany
[h] Division of Materials Science and Engineering, Boston University, Brookline, MA, 02446, USA
[i] Advanced Materials Center, Laboratory of Functional Materials, Faculty of Electronics, Telecommunications, and Informatics, Gdańsk University of Technology, Gdańsk, 80-233, Poland

HIGHLIGHTS

- This study compares 8 coatings from various research groups for 3000 h at 800 °C.
- MCO-coated steels exhibited >50-fold lower Cr evaporation than the uncoated steel.
- The lowest Cr evaporation was obtained for MCFAPS coating (2.1×10^{-10} $mgcm^{-2}s^{-1}$).
- MCO-coated steels have an at least 3x thinner Cr_2O_3 scale than the uncoated steel.
- Despite differences in the coating thickness and composition, the ASR is similar.

GRAPHICAL ABSTRACT

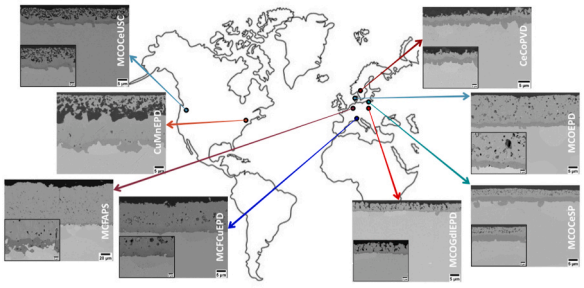

ARTICLE INFO

Keywords:
Solid oxide fuel cell
Interconnect
Coatings
Oxidation
Chromium evaporation
MCO coating

ABSTRACT

Ferritic stainless steel interconnects are used in solid oxide fuel cells; however, coatings are required to improve their performance. Although several types of coatings have been proposed, they have been scarcely investigated under similar conditions. This study compares the characteristics of uncoated Crofer 22 APU and eight different coatings on Crofer 22 APU for up to 3000 h at 800 °C. The coatings were deposited at various research laboratories around the world, and the experiments were performed at Chalmers University of Technology, Sweden. Cross-sections of the samples were analysed using scanning electron microscopy and energy-dispersive x-ray spectroscopy. The (Co,Mn)-based coated steels showed more than 50-fold lower chromium evaporation and at

* Corresponding author.
E-mail address: mareddy@chalmers.se (M.J. Reddy).

https://doi.org/10.1016/j.jpowsour.2023.232831
Received 23 December 2022; Received in revised form 3 February 2023; Accepted 14 February 2023

least 3 times thinner Cr_2O_3 scale thickness compared to uncoated steel. The coated steel samples showed lower area-specific resistance (ASR) values than the uncoated steel after 3000 h of exposure, irrespective of the coating thickness, composition and deposition method.

1. Introduction

Solid oxide fuel cells (SOFCs) are highly efficient electrochemical cells that are operated at high temperatures (550°–850 °C). The electrical efficiency of SOFCs has been reported as >60% [1], while in combined heat and power (CHP) mode, their efficiency is as high as 90% [2]. SOFCs are highly suitable for integration into the existing power grid due to their lower emissions levels, high efficiency, fuel flexibility, lack of moving parts, and silent operation. Single planar SOFCs produce a voltage of about 1 V per cell under typical operating conditions. Thus, multiple cells are stacked in series to generate a useable power output. Interconnects are used between the individual cells to act as current collectors, as well as to separate and direct the gas flows inside the cell.

Due to the challenges associated with the demanding operating conditions in SOFCs, such as stability during high-temperature operation and exposure to air and fuel atmospheres on either side, interconnect materials have stringent material selection criteria. The interconnects are typically made of ferritic stainless steel (FSS), which has the following combination of properties: low permeability to gases, high electrical conductivity, a coefficient of thermal expansion (CTE) that is similar to that of the other cell components and a low cost of manufacturing.

Upon exposure to high temperatures, the FSS forms a protective chromia layer that inhibits further oxidation of the steel and shows a relatively high conductivity in contrast other scales as alumina. This presents two major limitations for using chromia-forming FSS as interconnects. First, the thickness of the chromia scale increases over time, usually exhibiting parabolic oxidation kinetics, resulting in increased electrical resistance across the cell [3,4]. Moreover, the growth of the chromia scale can lead to spallation and cracking, resulting in the loss of electrical contacts. Second, the chromia scale interacts with humid air at high temperatures, resulting in the formation of volatile chromium species. These volatile Cr (VI) species interact with the cathodic materials at the oxygen-reducing sites and block them. This results in a decrease in the activity of the oxygen reduction reaction at the cathode, which is referred to in the literature as 'cathode poisoning' [5,6].

The most-effective way to reduce chromium evaporation is the application of protective coatings to the steel. Moreover, some protective layers are reported to reduce chromia scale growth [7–10], resulting in lower rates of degradation. Much research has been carried out on protective coatings, which differ in relation to their constituent elements, compositions and deposition techniques used. The interconnect coating types studied most often are: (a) perovskites; and (b) spinels. Perovskites, with the general formula of ABO_3, exhibit p-type electronic conduction in an oxidising environment and are usually stable under rather low oxygen partial pressures (low pO_2) [11]. Despite improvements, perovskite coatings represent ineffective barriers to chromium evaporation [12]. In contrast, spinels, with the general formula of AB_2O_4, have attracted interest owing to their ability to suppress chromium evaporation. Reddy et al. [13,14] have reported a 60-fold decrease in chromium evaporation from $(Co,Mn)_3O_4$ spinel-coated Crofer 22 APU steel, as compared to the uncoated steel. Moreover, spinels can be tailored to a specific application by altering the choices of A and B cations, thereby changing the properties of the spinel.

Petric et al. [15] have published a comprehensive overview of the conductive and thermal expansion properties of many different spinels, to identify spinel coatings that are better suited for interconnect applications. $(Co,Mn)_3O_4$-, $(Cu,Mn)_3O_4$-, and $(Ni,Fe)_3O_4$-based spinels with various dopants have been researched for interconnect applications. These spinels have been deposited using various methods, such as physical vapour deposition (PVD) [3,16–19], sol-gel dip-coating [20–23], electrophoretic deposition (EPD) [24–27], electroplating [28,29], screen printing [30,31], spray pyrolysis (SP) [32,33], inkjet printing [34,35], thermal co-evaporation [36,37] and atmospheric plasma spraying (APS) [38–42]. As of October 2022, more than 500 research papers with the keywords "interconnect" and "coating" have appeared in Scopus, and almost all of them are SOFC-related. The number of publications on this topic increased sharply around 2007 and since then, approximately 30 new papers have appeared annually. Most of these papers have investigated one specific coating composition in combination with a certain deposition technique. A few studies have been published in which different coatings have been compared, usually deposited using the same deposition technique [8,18,43], and some reports have compared the same coating deposited using different techniques [18,44]. However, it is difficult to compare the effectiveness of the coatings across the different reports due to the variations in testing conditions between the reports. Comparisons of coatings deposited using different methods on different substrates, such as Sanergy HT, Crofer 22 APU and 441, have been conducted in-situ [45] and ex-situ [46]. However, the aforementioned studies [45,46] focused on the area-specific resistance (ASR) of the coatings. Since chromium evaporation and oxide scale structure and growth are important for the interconnect, it is important to study coatings that are deposited using different methods.

In the present study, the authors from Chalmers University of Technology, Gothenburg, Sweden contacted 11 research laboratories in Europe, USA and Asia and proposed a comparative study. Furthermore, an invitation to participate in the present study was announced at the SOFC XVI Meeting in Kyoto, Japan. This work aims to provide data that would allow a direct comparison of the results obtained in different laboratories, and to provide baseline reference data for future studies. The coatings were deposited in various research laboratories using physical vapour deposition, sol-gel dip-coating, electrophoretic deposition and co-deposition, spray pyrolysis, and atmospheric plasma spraying on Crofer 22 APU. The studied parameters were chromium evaporation, mass gain and ASR, following exposure to 800 °C for up to 3000 h. The coated samples are characterised before and after the exposure using scanning electron microscopy (SEM) and energy-dispersive x-ray spectroscopy (EDX).

2. Experimental

2.1. Materials

The steel used as the base material for the various coatings in the present study was Crofer 22 APU with a thickness of 0.3 mm (composition presented in Table 1). All the coatings were deposited on the pre-cut steel sheets with a coupon size of 17 × 15 mm^2 and 15 × 15 mm^2. The coupons were attached to the steel frame with two 1-mm joints, resulting in a coating coverage of 99.8%. The pre-cut steel sheets were shipped to the seven participating laboratories, which used various deposition techniques and materials to apply the coating on both faces. The coating parameters were selected by the respective laboratories according to their previous experience. Most of the coatings had

Table 1
Chemical composition of Crofer 22 APU (in weight %).

Alloy	Fe	Cr	C	Mn	Si	Ti	La
Crofer 22 APU	Bal	22.92	0.004	0.38	0.01	0.06	0.07

undergone heat treatment in reducing and oxidising atmospheres for varying lengths of time. Table 2 provides comprehensive information about the coating, coating material, technique, and heat treatment, as well as further information related to the coating.

2.2. Exposures

The coated materials were shipped back to Chalmers University of Technology, where all the coupons were ultrasonically cleaned in acetone and ethanol for 20 min each, to remove any contaminants present on the surface. The samples were dried and weighed using a Mettler Toledo XP6 scale before starting the exposure. The coupons were exposed at 800 °C in tube furnaces with a continuous flow. To simulate the SOFC cathode-side atmosphere, the air was humidified with 3% H_2O. This was achieved by leading the air through a heated water bath (approximately 28 °C) that was further connected to a condenser maintained at a temperature of 24.4 °C, representing 3% H_2O in air. A porous SiC flow restrictor was positioned in front of the samples to ensure a uniform flow and to minimise the natural convection. The airflow was set at 6000 sml min^{-1} to ensure a flow-independent regime inside the reactor. The coupons were placed in an alumina holder along the direction of the airflow.

Two different types of exposures were performed: discontinuous mass gain exposures; and continuous chromium evaporation exposures. The exposures were performed in two types of tube furnaces; single-zone furnaces; and 3-zone furnaces. The 3-zone furnaces could accommodate up to 30 coupons, as compared to 6 coupons in the single-zone furnace. In the mass gain exposures, the coupons were removed at regular intervals from the furnace, cooled to room temperature, and the mass gain was recorded before the samples were placed in the furnace. At least six coupons were used for each mass gain exposure, and the exposure was performed for 3000 h. In the chromium evaporation exposures, three coupons of each type were used for each exposure. In-situ chromium evaporation was measured using the denuder technique devised by Froitzheim et al. [47]. The gas stream of the reactor containing vapourised chromium species was passed through a denuder tube coated with Na_2CO_3. The vapourised chromium species reacted with the Na_2CO_3 according to Equation (1).

$$Na_2CO_3(s) + CrO_2(OH)_2(g) \rightarrow Na_2CrO_4\ (s) + CO_2(g) \quad (1)$$

The denuder tubes were replaced at regular intervals without interrupting the exposure. The removed denuder tubes were leached with water, and the solutions were analysed in the Thermo Scientific Evolution 60S spectrometer, to determine the time-resolved chromium evaporation of the exposed coupons. To measure chromium evaporation, the uncoated Crofer 22 APU was exposed for 500 h at 800 °C, and the coated coupons were exposed for 1000 h at 800 °C.

2.3. SEM analysis

The cross-sections of the coated steels in as-received condition and exposed for 3000 h were prepared using a Leica TIC3X™ by broad ion beam (BIB) milling. The microstructure and chemical composition were characterised using the JEOL JSM-7800F Prime scanning electron microscope equipped with an Oxford Instruments energy-dispersive x-ray spectrometer.

2.4. Area-specific resistance measurements

ASR measurements were carried out ex-situ on the uncoated and coated coupons that were exposed for 3000 h. A sputter mask of 10 × 10 mm^2 was placed on the exposed coupon and a thin layer of platinum was sputtered on top using a sputter coater. After sputtering, a platinum paste (Metalor 6926) was applied to the sputtered area. The same procedure was carried out on the other side of the coupon. These coupons were further dried at 150 °C for 10 min, followed by a sintering step at 800 °C for 1 h. The resistance was measured at 800 °C using a 4-wire 2-point mode. A Keithley 2400 source meter was used for the measurement with the applied current set at 100 mA/cm^2. The resistance of each sample was measured at 800 °C. Subsequently the semi-conducting behaviour was assessed by measuring the ASR as the coupons cooled. A more-detailed description of the ASR measurement technique can be found elsewere [48].

3. Results and discussion

3.1. As-received coatings

Fig. 1 shows the SEM micrographs of the BIB-milled cross-sections of the coated Crofer 22 APU samples before exposure (i.e., the as-received coatings). Note that the magnification factors of the micrographs differ. The micrographs are arranged in order of coating thickness (Fig. 1, a-h). The thicknesses of the coatings are presented in Table 2 and range from 0.6 ± 0.1 μm to 93 ± 7 μm. All the coatings were received in oxidised form, with the exception of the CeCoPVD coating and MCFAPS coating which was partially oxidised. Nonetheless, the metallic CeCoPVD coating transforms upon oxidation to a $(Co,Mn)_3O_4$ spinel, owing to the diffusion of Mn from the steel substrate to the coating.

After application of the coating, except for the CeCoPVD and MCFAPS coatings, all the coated steels were subjected to different pre-treatments (Table 2). The coated samples that underwent pre-treatments are highlighted with a red border around the micrograph

Table 2
Specification of investigated coatings and deposition methods.

Coating	Composition	Thickness (μm)	Coating method	Pre-treatment	Lab	Ref
CeCoPVD	1.6% Ce 98.4% Co	0.6 ± 0.1	Physical vapour deposition	–	Chalmers University of Technology, Sweden	[14, 47,70]
MCOGdIEPD	Gd_2O_3 + $MnCo_2O_4$	2.2 ± 0.25	Electrophoretic deposition	Reduction: 2 h, 900°C, Ar + 10% H_2; Oxidation: 4 h, 900°C, static air	AGH University of Science and Technology, Poland	[7,71]
MCOCeSP	MCO + 5% CeO	3.3 ± 0.8	Spray pyrolysis	Binder burnoff 800°C (30 min)	Gdańsk University of Technology, Poland	[50, 72,73]
MCOCeUSC	$(Mn,Co)_{2.98}O3.98$ + 0.02 CeO	5.2 ± 0.7	Sol-gel Ultrasonic spray coating (USC)	Reduction: 5 h, 850°C, H_2; Oxidation: 1 h, 1000°C, air	Pacific Northwest National Laboratory, USA	[74]
CuMnEPD	$CuMn_{1.8}O_4$	14 ± 2.6	Electrophoretic deposition	Reduction: 24 h 1000°C in forming gas (Ar + 2% H_2), 100 h in air at 850 °C	Boston University, USA	[26, 75,76]
MCOEPD	$MnCo_2O_4$	17 ± 2.2	Electrophoretic deposition	Reduction: 1 h, 1000°C, 4%H2–N2 (dry); Oxidation: 5 h, 800°C, air (ambient)	Technical University of Denmark, Denmark	[49, 77]
MCFCuEPD	$Mn_{1.2}Co_{1.2}Fe_{0.3}Cu_{0.3}O_4$	18 ± 3.5	Electrophoretic co-deposition	Reduction: 2 h, 1000°C, flowing Ar/H_2 (2 vol%); Oxidation: 2 h, 900°C, static air	Politecnico di Torino, Italy	[24, 78]
MCFAPS	MCF	93 ± 7	Atmospheric plasma spraying	–	Forschungszentrum Jülich, Germany	[41, 42]

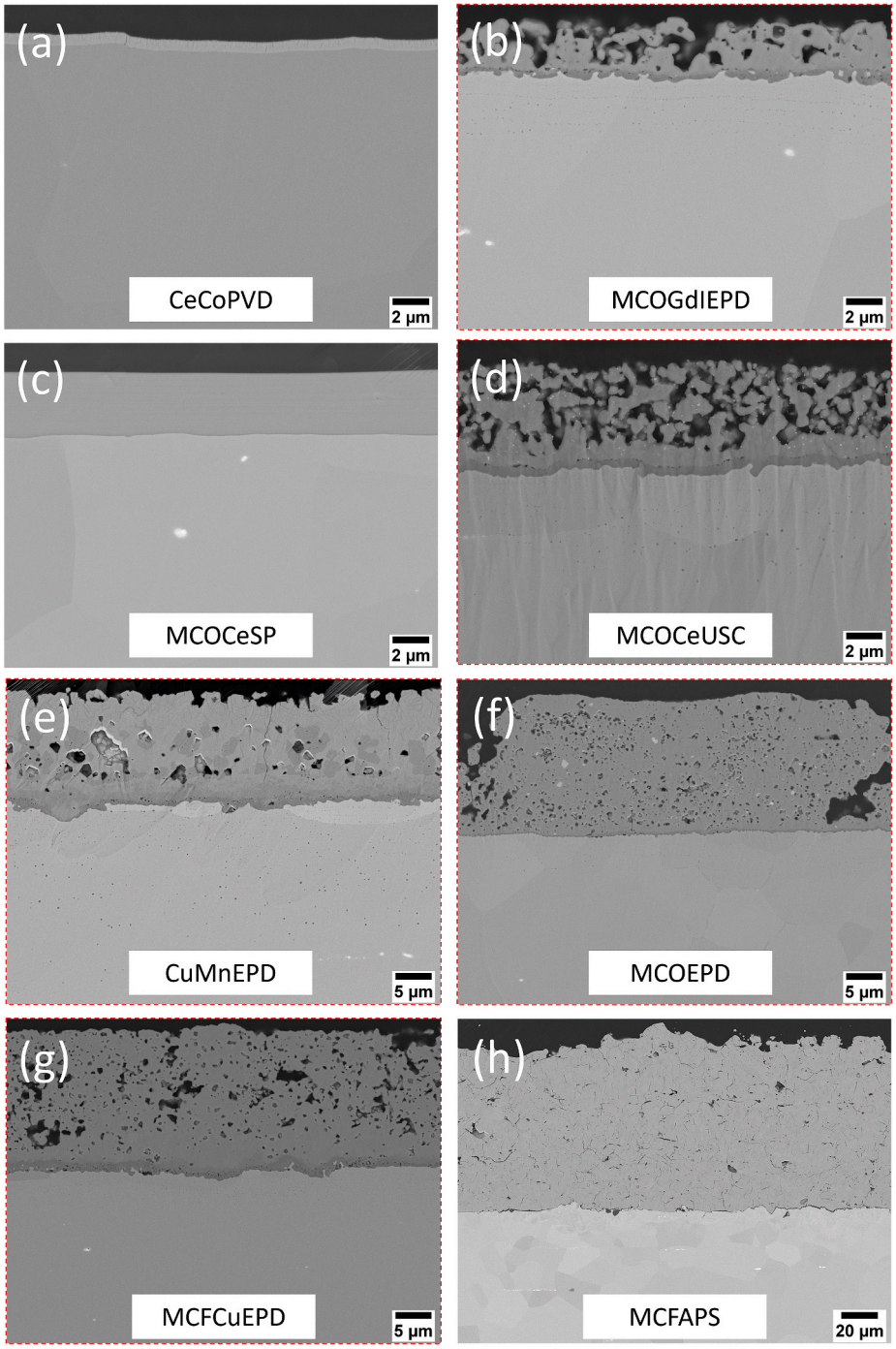

Fig. 1. BIB-milled cross-sections of Crofer 22 APU coated with: (a) CeCoPVD; (b) MCOGdIEPD; (c) MCOCeSP; (d) MCOCeUSC; (e) CuMnEPD; (f) MCOEPD; (g) MCFCuEPD; and (h) MCFAPS (as-received).

in Fig. 1. Although the type of pre-treatment varied across the different laboratories, it is always performed in a low pO_2 atmosphere, followed by an oxidising atmosphere. Talic et al. [49] have shown that the reduction and re-oxidation of the electrophoretic deposition (EPD) coating results in denser coatings compared to oxidation in air only. Furthermore, Talic et al. [49] have observed that the chromium evaporation rate is 3-fold lower at 800 °C on the denser coatings formed by the two steps of pre-treatment. As a result of the pre-treatment, a chromia scale is formed at the metal-oxide interface on the pre-treated coated steel. The thickness of the chromia scale formed during the experiment presented here is influenced by the temperature and time of the pre-treatment. The pre-treatments in air of the coated samples shown in Table 2 were conducted at temperatures in the range of 800°–1000 °C for 2–100 h. All the coated samples, with the exceptions of the CeCoPVD and MCOCeSP coatings, exhibited coating porosity. The coatings produced by spray pyrolysis (MCOCeSP) require pre-treatment in air to burn off organic residuals after coating deposition [50]. In the present work, the MCOCeSP coatings were pre-treated at 800 °C for 0.5 h before the exposure. Although EPD coating followed by the heat-treatment steps resulted in a dense coating, some porosity was observed in the micrographs. However, the porosity was mostly clustered to the coating-air interface.

Fig. 2 shows the EDX maps of the coatings deposited on Crofer 22 APU before the exposure. In Fig. 2, b, d, e, f, and g, a chromia scale is

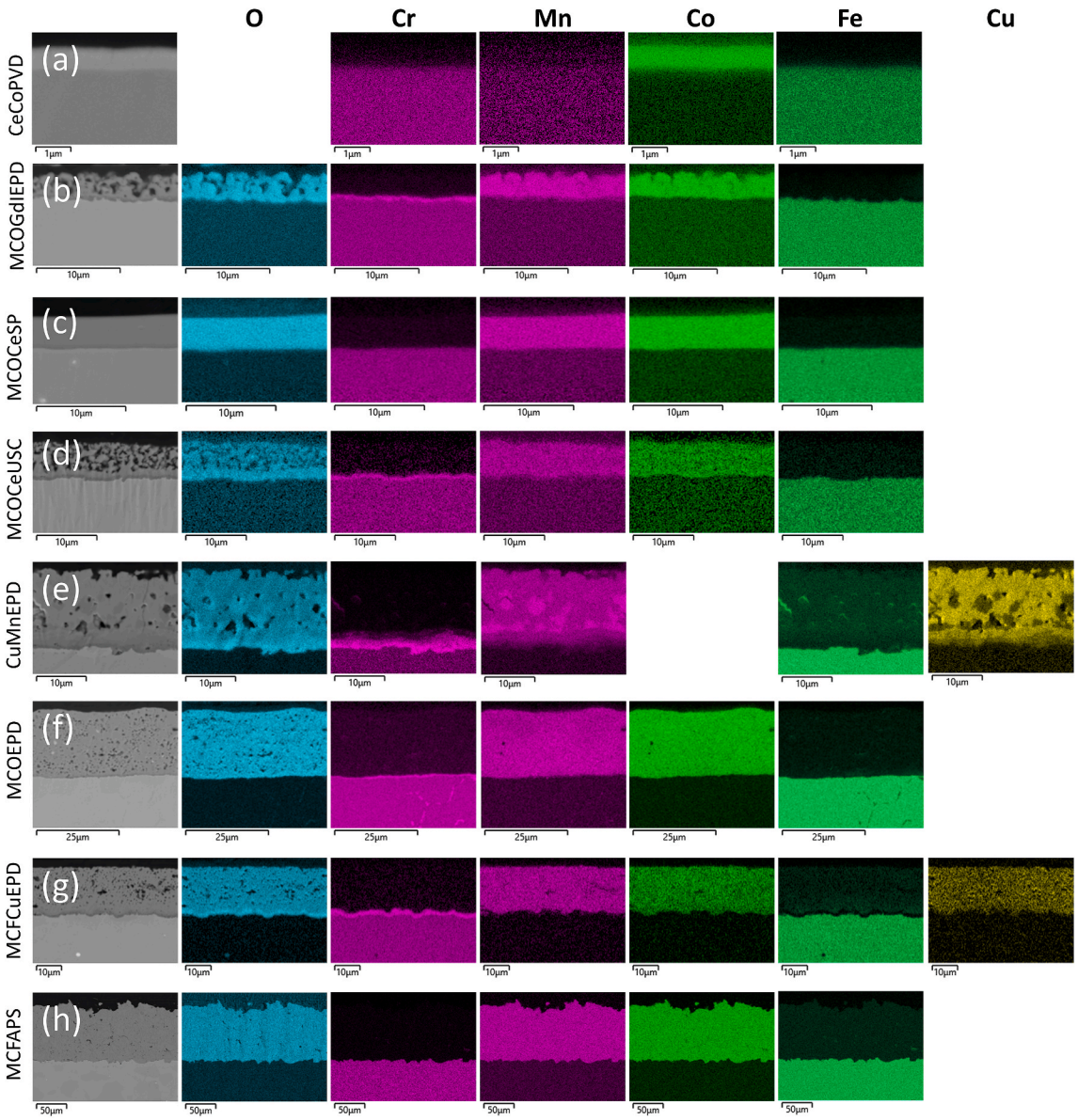

Fig. 2. EDX maps of the BIB-milled cross-sections of Crofer 22 APU coated with: (a) CeCoPVD; (b) MCOGdIEPD; (c) MCOCeSP; (d) MCOCeUSC; (e) CuMnEPD; (f) MCOEPD; (g) MCFCuEPD; and (h) MCFAPS (as-received condition after pre-treatments, if any. Refer to Table 2).

observed at the metal-oxide interface, as expected. Moreover, in the coated samples that underwent pre-treatment, internal oxidation of Ti is visible in the substrate below the metal-oxide interface in Fig. 1; this is a commonly observed feature of oxidised Crofer 22 APU. All the coatings, with the exception of the CuMnEPD coating, are based on manganese cobalt oxide (MCO), with various additions. MCOCeSP contains a small amount of Cu due to unknown contamination, MCFCuEPD has 1.5 atomic % (at%) Cu and 1.5 at% Fe added, and MCFAPS has 1.5 at% Fe added to the MCO. In addition to the MCO and dopants, reactive elements such as Ce, Gd, and Zr are present in some coatings. Reactive elements in the coatings are known to be highly effective at improving the high-temperature oxidation behaviour of the substrate.

3.2. Chromium evaporation

The chromium evaporation profiles of the uncoated and coated Crofer 22 APU samples exposed at 800 °C in air +3% H_2O for up to 1000 h are presented in Fig. 3. Fig. 3a shows the cumulative levels of chromium evaporation and Fig. 3c shows the rates of chromium evaporation for the selected materials. Fig. 3, b and d show the zoomed-in regions of Fig. 3, a and c, respectively. All the coated Crofer 22 APU's exhibited substantially lower levels of chromium evaporation than the uncoated Crofer 22 APU. This indicates that the studied coatings act as barriers to chromium evaporation, albeit with very different efficiencies.

The CuMnEPD coating reduced chromium evaporation 2–5-fold, while the CoMnAPS coating reduced chromium evaporation 100-fold, as compared with the uncoated steel. Overall, the coatings based on Co and Mn seemed to be more effective than the coatings based on Cu and Mn. This is in line with the findings of Tomas et al. [51], who showed that chromium evaporation from Cu-coated steel was similar to that from uncoated steel at 850 °C. Moreover, Farzin et al. [52] have shown that the application of a Cu–Mn contact paste to MCO-coated Crofer 22 APU results in an increase in the fracture toughness of the contact layer due to inter-diffusion of the Cr_2O_3 layer, coating and contact paste. Furthermore, Farzin et al. [52] have confirmed that the rate of diffusion of Cr into a $(Cu,Mn)_3O_4$ spinel is lower at 750 °C than at 850 °C. Nevertheless, such a Cu coating is highly effective at inhibiting chromium evaporation at 650 °C [18]. Based on these results, it can be concluded that Cu-based

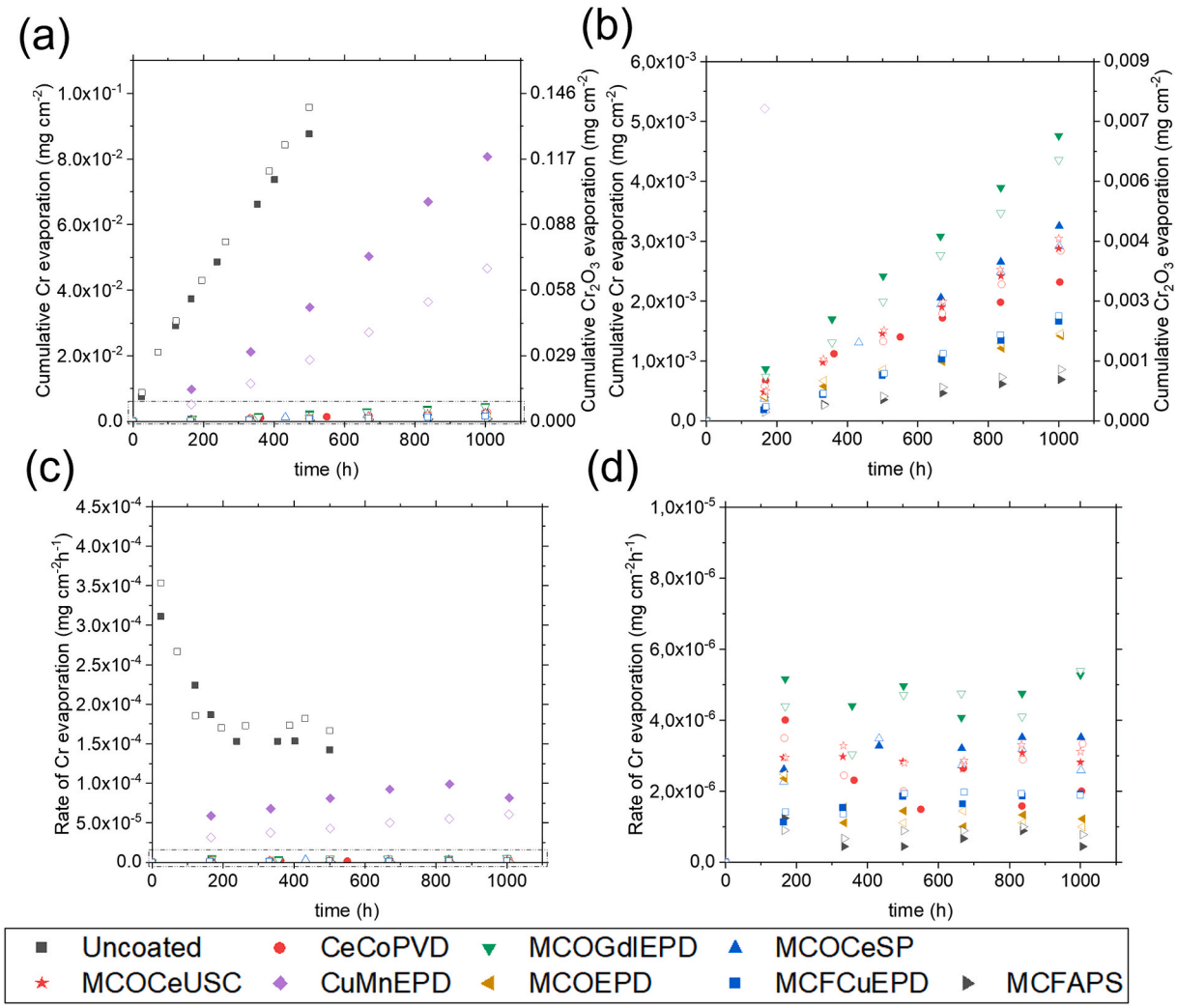

Fig. 3. (a) Cumulative chromium evaporation and (c) Rate of chromium evaporation of the uncoated and coated steels exposed to 800 °C in air + 3% H_2O for up to 1000 h isothermally. b and d, Zoomed-in regions of the cumulative chromium evaporation and rate of chromium evaporation, respectively. Open and filled symbols represent two individual exposures.

coatings are more suitable for use at lower temperatures, at least in terms of chromium evaporation.

All the coatings based on MCO showed a 50–100-fold decrease in chromium evaporation compared with the uncoated steel after 500 h of exposure. Of the MCO-based coatings, the MCOGdIEPD-coated samples exhibited the highest chromium evaporation, which was still 50-times lower than that for the uncoated samples. This may be attributable to MCOGdIEPD having a thinner coating and higher porosity compared to the other coatings. The data show that the samples with the lowest chromium evaporation, MCFAPS, MCFCuEPD, and MCOEPD have coatings with thicknesses over 15 μm, indicating a somewhat beneficial effect of thicker coatings. However, this effect seems to be relatively small as the coating thickness varied from 1 μm to 93 μm between CeCoPVD and MCFAPS coating, the chromium evaporation changed only by a factor of 2. The Cr evaporation rates for all the coated steels (except CuMnEPD) were constant throughout the exposure. The rate of chromium evaporation of the uncoated Crofer 22 APU decreased during the first 200 h of the exposure; this type of behaviour has been reported earlier [53]. This is due to the diffusion of the Mn in the steel to the oxide layer, resulting in the formation of a $(Cr,Mn)_3O_4$ spinel.

Table 3 compares the present data, with the reported values of chromium evaporation rates (10^{-10} mg cm^{-2} s^{-1}) for uncoated and coated steels at 800 °C. Due to different analysis techniques, differences in flow rate, geometry and humidity, there are significant differences in the reported values. Nevertheless, most of the reported values for the uncoated ferritic steels seem to be in the range of 2–5 x 10^{-8} mg cm^{-2} s^{-1}. In contrast, most of the reported values for the coated steels are below the range of 10^{-9} mg cm^{-2} s^{-1}.

3.3. Oxidation kinetics

Fig. 4 shows the oxidation kinetics in terms of mass gain for the uncoated and coated Crofer 22 APU samples exposed at 800 °C in air +3% H_2O for up to 3000 h. Fig. 4b is the zoomed-in version of Fig. 4a. The MCFAPS and CeCoPVD coatings were not fully oxidised due to the absence of a pre-treatment. To allow comparisons of the mass gain curves of these coatings, the mass gains after 1 h (0.93 mg/cm^2 and 0.24 mg/cm^2 for MCFAPS and CeCoPVD, respectively) are subtracted in the plot shown in Fig. 4. MCFAPS showed the highest mass gain of 2.49 ± 0.07 mg/cm^2 after 3000 h. The initial steep increase in mass observed for the MCFAPS coating during the first 200 h indicates that 1 h of oxidation at 800 °C is not sufficient to oxidise fully the coating, probably owing to the greater thickness of the deposited coating. Grünwald et al. [40,54] studied phase transformations in this coating with X-ray diffraction and thermogravimetry. The authors studied the phase distribution as a function of time and temperature and found substantial amounts of MO (M = Co, Fe, Mn) after 100 h exposure at 700 °C. The subsequent oxidation of MO (in the as-received MCFAPS coating) to

Table 3
Cr evaporation rate (10^{-10} mg cm^{-2} s^{-1}) from the present work and literature data reported at 800 °C at using various techniques. The data are obtained in different flow regimes, and there are significant differences in the gas velocity between the different studies. The evaporation rate is calculated by dividing accumulated Cr evaporation by duration of the exposure.

Material	Coating	Temp (°C)	Time(h)	Details	Rate of Cr evaporation 10^{-10} mg cm^{-2} s^{-1}	[Ref]
Crofer 22 APU	–	800	1000	Air + 1.88% H_2O	400	[79]
Crofer 22 APU	–	800	500	Air + 3%H_2O	110	[80]
Crofer 22 APU	–	800	24–96	Air + 7%H_2O	160	[81]
Crofer 22 APU	–	800	500	Air + 3%H_2O	505	This work [49],
Crofer 22 APU	–	800	1000	Air + 2%H_2O	170	[82]
Crofer 22 APU	MCO	800	500	Air + 3%H_2O	25	[80]
Crofer 22 APU	MCF	800	1000	Air + 2%H_2O	2.4	[82]
Crofer 22 APU	CeCoPVD	800	1000	Air + 3%H_2O	7.1	This work
Crofer 22 APU	MCOGdIEPD	800	1000	Air + 3%H_2O	12.5	This work
Crofer 22 APU	MCOCeSP	800	1000	Air + 3%H_2O	8.5	This work
Crofer 22 APU	MCOUSC	800	1000	Air + 3%H_2O	8.25	This work
Crofer 22 APU	CuMnEPD	800	1000	Air + 3%H_2O	175	This work
Crofer 22 APU	MCOEPD	800	1000	Air + 3%H_2O	4	This work
Crofer 22 APU	MCFCuEPD	800	1000	Air + 3%H_2O	4.4	This work
Crofer 22 APU	MCFAPS	800	1000	Air + 3%H_2O	2.1	This work
Crofer 22 APU	Co	800	1000	Air + 1.88% H_2O	0.9	[79]
Crofer 22 APU	Cu	800	1000	Air + 1.88% H_2O	2	[79]
Crofer 22 APU	Ni	800	1000	Air + 1.88% H_2O	1	[79]
AISI 441	–	800	500	Air + 3%H_2O	660	[14]
AISI 441	–	800	24–96	Air + 7%H_2O	250	[81]
AISI 441	–	800	96	O2 – 5% H_2O	2000	[83]
AISI 441	CeCo	800	1000	Air + 3%H_2O	7	[14]
AISI 444	–	800	500	Air + 3%H_2O	920	[14]
AISI 444	CeCo	800	1000	Air + 3%H_2O	8.8	[14]
AISI 409	–	800	500	Air + 3%H_2O	669	[14]
AISI 409	CeCo	800	1000	Air + 3%H_2O	9.1	[14]
AISI 430	–	800	500	Air + 3%H_2O	555	[14]
AISI 430	–	800	96	O2 – 5% H_2O	236	[84]
AISI 430	–	800	24	Air + 10% H_2O	1000	[85]
AISI 430	–	800	100	Air + 3%H_2O	45	[86]
AISI 430	–	800	100	Ar + 17% H_2O	200	[87]
AISI 430	MCO	800	24	Air + 10% H2O	50	[85]
AISI 430	MCO	800	96	O2 – 5% H_2O	112	[84]
AISI 430	TiCrAlYO	800	275	Ar + 17% H_2O	7	[87]
AISI 430	CeCo	800	1000	Air + 3%H_2O	10.8	[14]

M_3O_4 leads to the high mass gain presented in Fig. 4. Furthermore, it results in a volume expansion that closes typical cracks present in APS coatings leading to gas tight layers [40]. The samples coated with MCFCuEPD, MCOGdIEPD and MCOCeUSC exhibited the lowest mass gains of all the coated samples. The mass gains of these coated samples after 3000 h at 800 °C were 0.20 ± 0.02 mg/cm^2, 0.27 ± 0.02 mg/cm^2, and 0.24 ± 0.01 mg/cm^2, respectively. All of these coated samples were pre-treated in air at temperatures >900 °C. It is reasonable to assume that the higher temperature promoted the formation of a more-protective Cr_2O_3 scale. This effect may be attributable to a higher level of purity of the Cr_2O_3 scale. Furthermore, Sabioni et al. [55] have demonstrated the formation of coarser-grained Cr_2O_3 at higher temperature. A lower grain boundary density is expected to reduce ionic transport and, thus, a scale formed at higher temperature is expected to grow more slowly. The three coatings discussed above have different coating thicknesses, in the range of 2.2–18.0 μm. All of these coatings are based on MCO coatings, although the MCFCuEPD coating comprises MCO doped with Fe and Cu. The other two coatings, MCOGdIEPD and MCOCeUSC, contain the reactive elements Gd and Ce, respectively. Due to various parameters related to the coating composition and thickness, as well as pre-treatment time and temperature, it is difficult to compare these coatings. The measured mass gains do not correlate with the chromia scales observed after 3000 h of exposure, as some part of the chromia scale is already formed during the pre-treatment step, which also varied among these coated steels.

The samples coated with MCOEPD, MCOCeSP, and CeCoPVD can be grouped together with respect to their mass gains. The mass gains after 3000 h at 800 °C were 0.54 ± 0.006 mg/cm^2, 0.63 ± 0.01 mg/cm^2, and 0.66 ± 0.01 mg/cm^2, respectively. The mass gains of these coated samples were more than twice those of the coated samples that were pre-treated in air at temperatures >900 °C. MCOEPD was pre-treated for 5 h at 800 °C and showed the least mass gain of the MCOEPD-, MCOCeSP-, and CeCoPVD-coated samples. All three coated samples examined here contained the reactive elements Ce and/or Zr in their coatings. In the MCOEPD coating, Zr appeared in the coating powder during the milling of the MCO powder using Zr balls. The thicknesses of the coatings were: for MCOEPD, 17 ± 2 μm; for MCOCeSP, 3.3 ± 0.8 μm; and for CeCoPVD, 0.6 μm (although after oxidation, it was increased to about 1.0 μm). It is possible that either the thicker coating on MCOEPD or the pre-treatment in air for 5 h resulted in the lower mass gain for MCOEPD, as compared to MCOCeSP and CeCoPVD. Moreover, it is possible that the higher concentrations of reactive elements in MCOCeSP, as compared to CeCoPVD, did not influence, either positively or negatively, the mass gain. These results are in line with the study of Reddy et al. [56], in which it was found that an increase in the Ce thickness of the Ce/Co coating from 10 nm to 50 nm did not lower the oxidation kinetics at 800 °C.

The mass gain of CuMnEPD after 3000 h at 800 °C was 1.19 ± 0.11 mg/cm^2. The mass gain of the uncoated Crofer 22 APU after 3000 h at 800 °C was 1.04 ± 0.11 mg/cm^2. Although the measured mass gain of CuMnEPD was higher, this result is misleading. Uncoated Crofer 22 APU exhibits a mass loss due to Cr evaporation, which is approximately 0.71 mg/cm^2 after 3000 h, while the corresponding value for CuMnEPD is 0.28 mg/cm^2. The remainder of the coated samples exhibited such low Cr evaporation rates that the effect on mass gain was negligible. The chromia scale thicknesses of the uncoated and CuMnEPD steels will be

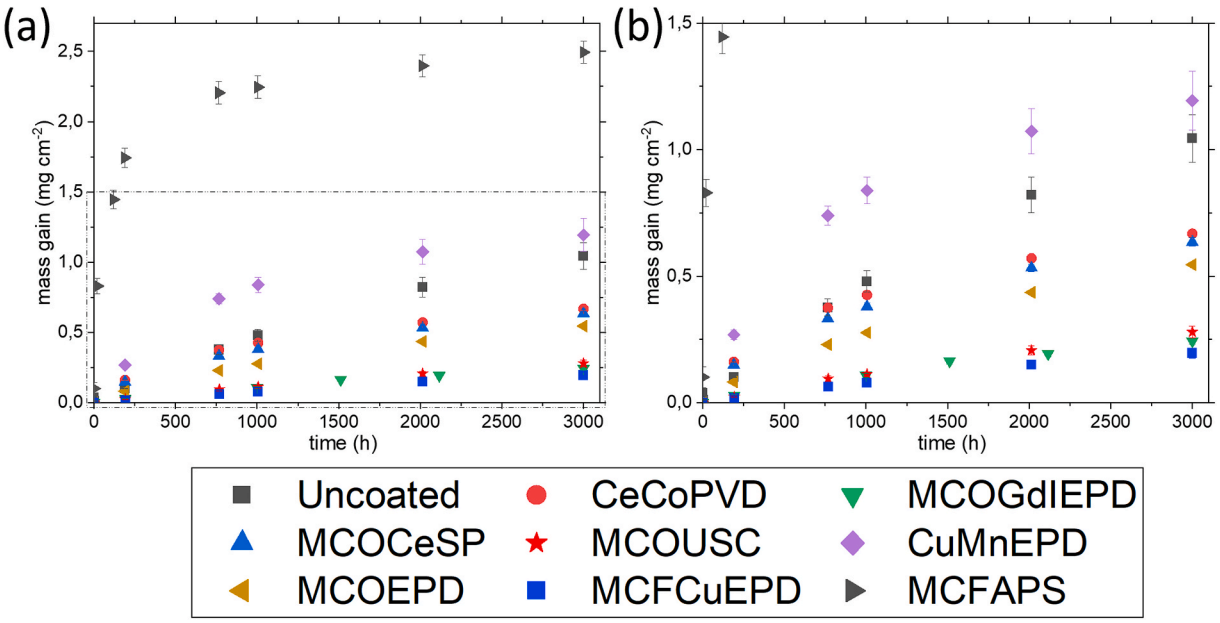

Fig. 4. (a) Net mass gain as a function of time for the uncoated and various coated Crofer 22 APU, exposed for 3000 h at 800 °C in air + 3% H_2O. Error bars represent standard deviations. (b) Zoomed-in region of the net mass gain plot.

discussed in the next section.

Although the experiments were performed under similar conditions, it is difficult to compare the oxidation performances of different coated samples owing to the different heat treatments experienced before the exposure. However, it is possible to state that all of the coated steels exhibited lower oxidation kinetics than the uncoated steels after 3000 h of exposure.

3.4. Microstructure

Fig. 5 shows the SEM micrographs and EDX maps for the BIB-milled cross-sections of the uncoated Crofer 22 APU samples exposed for 3000 h at 800 °C. The SEM micrograph shows the presence of two distinct oxide layers. Based on the EDX maps, it appears that the top of the oxide scale is rich in both Cr and Mn, identified as a $(Cr,Mn)_3O_4$ spinel, while underneath the spinel lies a Cr-rich layer, Cr_2O_3. The formation of a $(Cr,Mn)_3O_4$ spinel and a Cr_2O_3 scale in an Mn-containing FSS has been reported earlier [57,58]. After 3000 h, the oxide scale has a thickness of 8.7 ± 0.56 μm, of which more than 80% appears to be the chromia scale. Some Mn-rich areas are observed in the chromia scale at the metal-oxide interface, as has also been reported earlier [59].

Fig. 6 shows the SEM micrographs of the BIB-milled cross-sections of the coated Crofer 22 APU samples exposed for 3000 h at 800 °C. Table 4 presents the thicknesses of the Cr rich oxide scales, calculated based on the contrast differences in the back-scattered electron (BSE) images. On some of the coated samples, such as CoCePVD, MCOCeSP, MCOEPD and MCFAPS, a distinct chromia scale was observed. In other cases, a Cr-enriched layer at the coating-chromia scale interface (see below) was found. Since it was difficult to distinguish those layers, the thickness of chromia layer and Cr enriched layer is presented in Table 4. The correlation between the mass gain presented in Fig. 4 and chromia scale thickness presented in Table 4 is not straightforward. Although there is some correlation, for example, MCOGdIEPD has the thinnest chromia scale and a low mass gain, there are the following complications: (i) The mass changes during the pre-treatment procedures are not accounted for in the mass gain data plotted in Fig. 4. (ii) The presence of the chromium enriched layer (iii) The observed mass gain of the MCFAPS coating is significantly influenced by the oxidation of the coating. The micrographs in Fig. 6 have different magnifications, while the inserts in the micrographs are at the identical magnification for all the specimens, to allow for easier comparison. All of the coated steels showed the presence of a continuous oxide scale, with no signs of spallation. Moreover, the

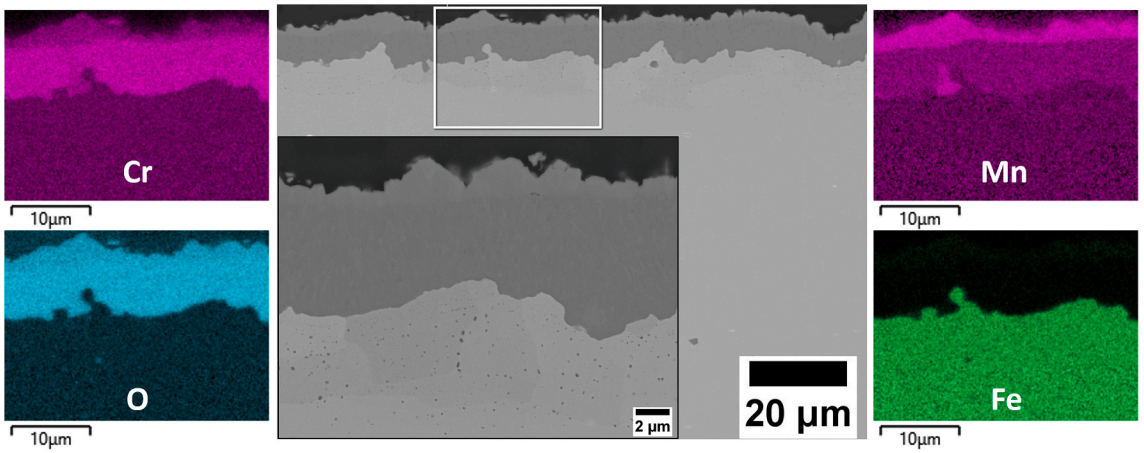

Fig. 5. BIB-milled cross-sectional micrographs and EDX maps of the uncoated Crofer 22 APU exposed for 3000 h at 800 °C in air +3% H_2O.

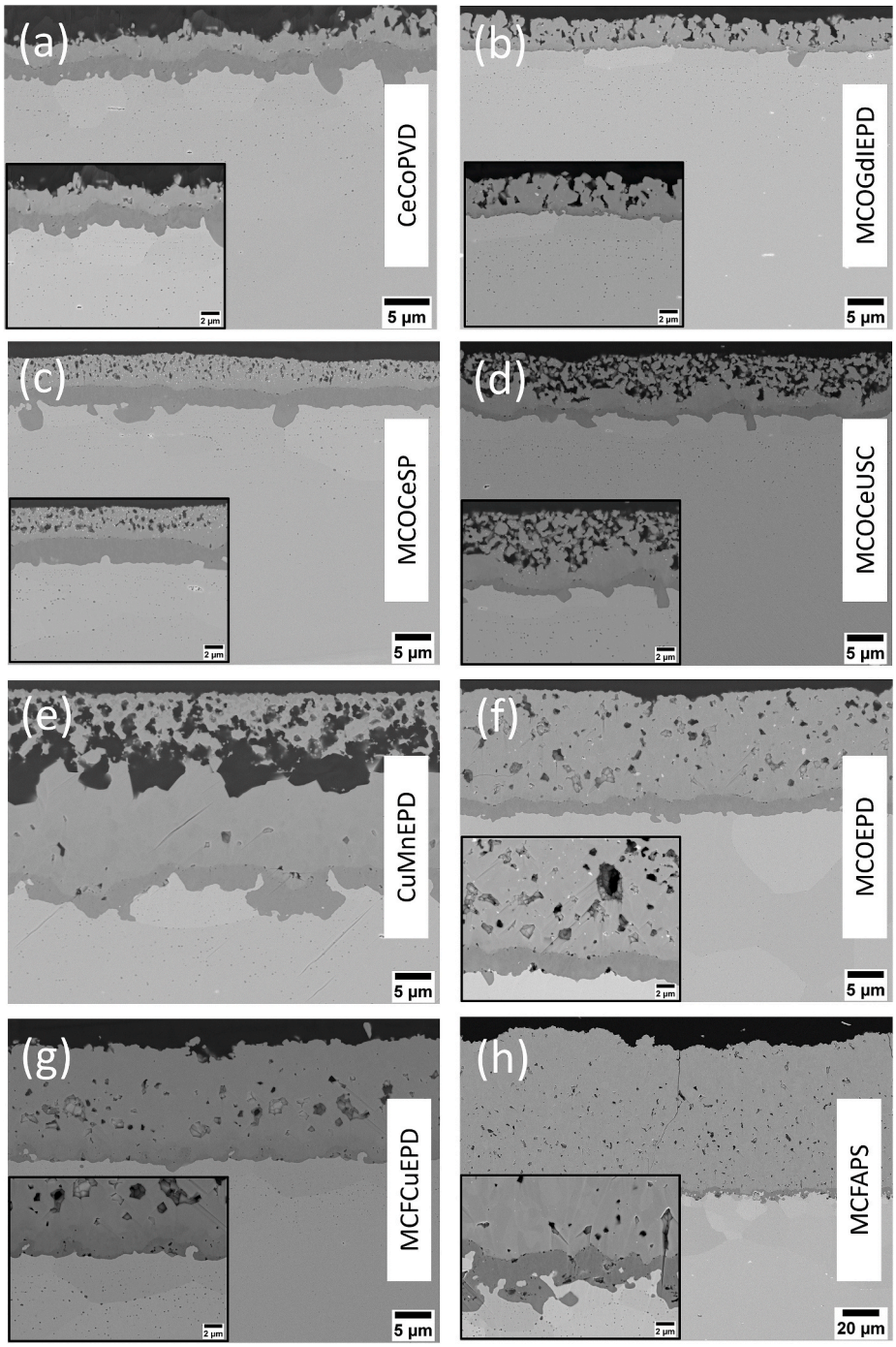

Fig. 6. BIB-milled cross-sections of Crofer 22 APU coated with: (a) CeCoPVD; (b) MCOGdIEPD; (c) MCOCeSP; (d) MCOCeUSC; (e) CuMnEPD; (f) MCOEPD; (g) MCFCuEPD; and (h) MCFAPS. The samples were exposed for 3000 h at 800 °C in air +3% H_2O.

coated steels displayed a similar oxide scale structure, with the coating on the top and a chromia scale at the metal-oxide interface. The thickness of the chromia scale varied between the coated steels. Due to the different pre-treatments prior to the exposure, the chromia scale thicknesses do not correlate with the mass gains. Fig. 7 shows the EDX maps in the BIB milled cross-sections of the coated Crofer 22 APU exposed for 3000 h in air with 3% H_2O. The micrographs and EDX maps are presented in the same order according to the thickness of the coating material.

Some of the coated steels showed a clear interface between the chromia scale and the coating after exposure to 800 °C for 3000 h. However, the MCOGdIEPD-, MCOCeUSC-, CuMnEPD-, and MCFCuEPD-coated samples showed a mixed layer of chromia scale and the coating. The presence of such mixed layers has been reported earlier and linked to an increase in the ASR [60,61]. Despite undergoing a similar coating process and having similar coating elements, the MCOEPD-coated steel

Table 4
Cr rich oxide scale thickness determined by the contrast differences in the back-scattered electron micrographs and EDX maps.

Coating	Chromia thickness (μm)	Min (μm)	Max (μm)
Uncoated	8.7[a]	5.7	10
CeCoPVD	2.8	0.9	5
MCOGdIEPD	1.2[b]	0.3	1.4
MCOCeSP	2.8	1.7	4.7
MCOCeUSC	1.9[b]	0.9	3.6
CuMnEPD	Continuous Cr gradient		
MCOEPD	2.7	1.5	3.2
MCFCuEPD	2.3[b]	1.2	3.3
MCFAPS	2.9	0.4	6.2

[a] Refers to Cr_2O_3 plus $(Cr,Mn)_3O_4$ layer.
[b] Estimated thickness for Cr_2O_3 plus Cr rich intermediate layer measured with the help of EDX maps shown in Fig. 7 and micrographs shown in Fig. 6.

did not show the presence of a Cr-rich mixed layer. The major differences between the MCOEPD coating and MCFCuEPD coating were the addition of Fe and Cu elements and the pre-treatment temperature. The MCFCuEPD coating was pre-treated in air at 900 °C for 2 h, while the MCOEPD coating was pre-treated in air at 800 °C for 5 h. Similarly, the coated samples MCOGdIEPD, MCOCeUSC, and CuMnEPD were pre-treated in air at temperatures >850 °C for various times. The high pre-treatment temperatures employed in the coating processes might lead to Cr diffusion into the spinel coating. Heat treatment is normally required for processes that use conventional wet ceramic techniques, such as EPD, to remove organic binders and to sinter deposited particles, which is not the case for APS, PVD or other thin-film deposition methods.

All the coatings exhibited some porosity. However, the degree of porosity varied between the coatings. The CeCoPVD coating and MCOCeSP coating exhibited no porosity in the as-received forms (Fig. 1). The MCFAPS coating contains microcracks that are visible at higher magnification (not shown) but not visible in Fig. 1. However, after 3000 h of exposure, some porosity was observed in the coatings. The porosity on the CeCoPVD coating was evenly spread throughout the coating. In contrast, the outer part of the MCOCeSP coating was highly porous, while the inner part was completely dense. Thus, a barrier existed between the chromia scale and the atmosphere, preventing chromium evaporation. Similar to the MCOCeSP coating, the MCOGdIEPD coating and MCOCeUSC coating showed porosity towards the coating air interface, as well as a dense coating at the chromia-coating interface. Among the coated steels that showed low-level chromium evaporation,

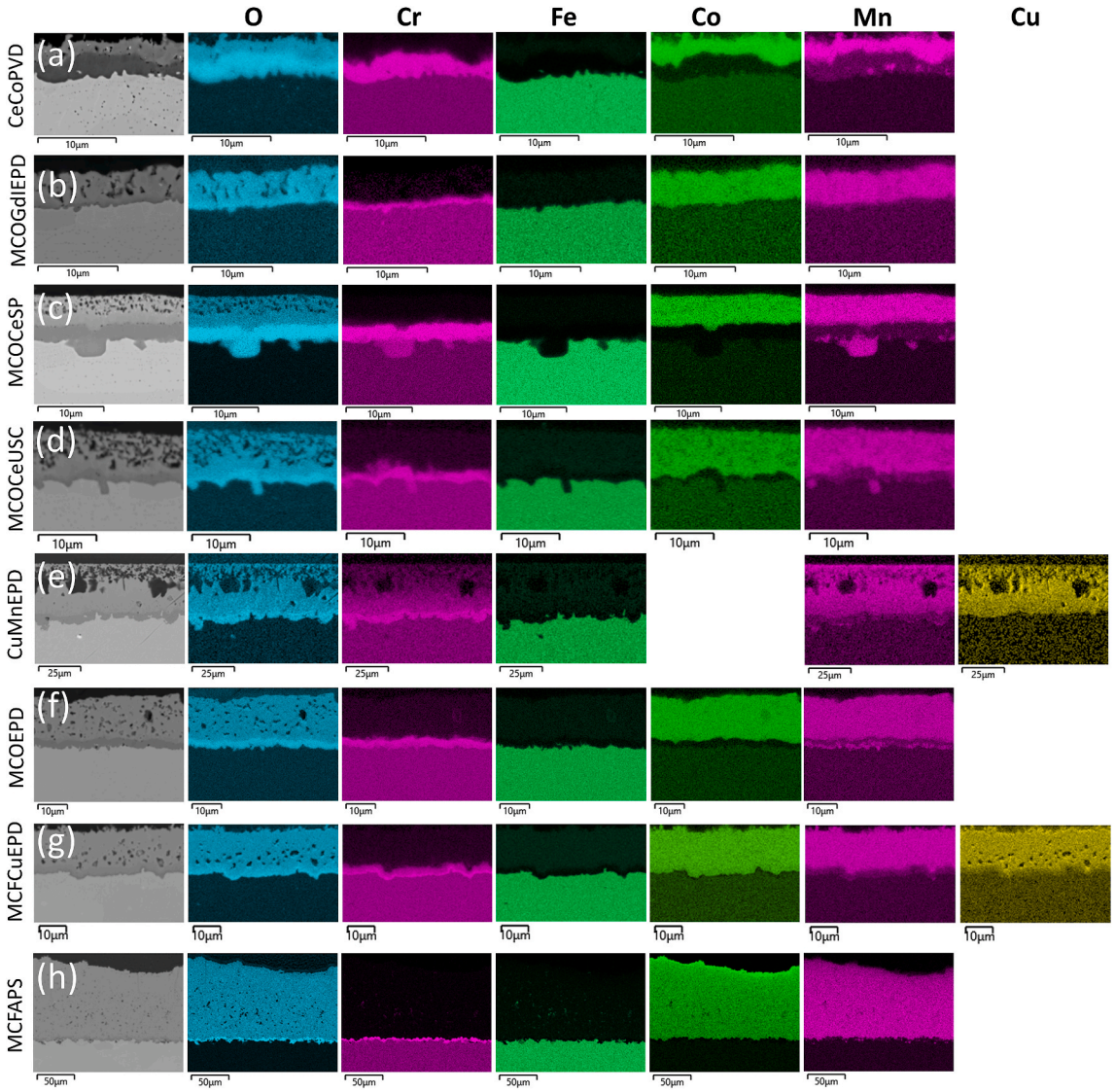

Fig. 7. EDX maps of the BIB-milled cross-sections of uncoated Crofer 22 APU (a), and Crofer 22 APU coated with: (b) CeCoPVD; (c) MCOGdIEPD; (d) MCOCeSP; (e) MCOCeUSC; (f) CuMnEPD; (g) MCOEPD; (h) MCFCuEPD; and (i) MCFAPS. The samples were exposed for 3000 h at 800 °C in air +3% H_2O.

MCOGdIEPD had the highest level of chromium evaporation (albeit 50-times lower than the uncoated sample), which is attributed to a higher porosity, possibly in combination with a thinner coating.

The reactive elements present in the coatings are visible in the BSE micrographs in Fig. 6. They appear as bright particles in the coating owing to the large atomic masses of these elements. The Ce-rich particles in CeCoPVD coating were spread throughout the coating and were not prominently visible due to the small size of the precipitates sparsely distributed throughout the coating. In the MCOGdIEPD coating, Gd-rich particles were visible in coating. Brylewski et al. [7] studied the MCOGdIEPD coating with transmission electron microscopy and found that Gd-rich particles are mostly found at the chromia-coating interface resulting in improved adhesion of the coating. Furthermore, Ce-rich particles were prominently evident in the MCOCeSP and MCOCeUSC coatings, probably due to higher concentrations of the reactive elements in the coating. Similarly, Ce and Zr were visible in the MCOEPD coating as bright particles. The commonly suggested hypothesis for the mechanism of reactive elements on chromia formers is that the reactive elements end up at the grain boundaries of the chromia scale and block the outward diffusion of Cr^{+3} ions, thereby reducing chromia scale growth and shifting the oxide scale growth direction from outward (Cr^{+3} transport) to inward (O^{2-} transport). Reactive element coatings [62–64] and reactive element-doped coatings [8,9,65,66] have been extensively studied in the SOFC context, and a significant reduction of chromia scale growth has often been reported. However, it is interesting to find that the reactive elements are mostly visible in the coating material rather than in the chromia scale after 3000 h of exposure. It is possible that the reactive element particles observed in the coating are excess material, while the reactive element particles in the grain boundary of the chromia scale are not visible due to the limited resolution of the SEM. The two coated samples, MCOCeSP and CeCoPVD, which had similar starting conditions, showed similar oxidation kinetics (Fig. 4). However, the amount of reactive elements in the coating was significantly higher in MCOCeSP coating than in the CeCoPVD coating, as can be seen in the SEM micrographs in Fig. 6, a and c.

The CuMnEPD-coated Crofer 22 APU steel exhibited a thinner chromia scale than the uncoated Crofer 22 APU steel, while the measured mass gain reported in Fig. 3 is higher for the CuMnEPD-coated steel. This is due to the high mass loss of the uncoated Crofer 22 APU due to chromium evaporation, as explained above. Significant outward diffusion of Cr was observed for the CuMnEPD-coated Crofer 22 APU. After 3000 h, the EDX maps (Fig. 7e) showed that the Cr signal was visible even at the coating-air interface. This accords with the finding that CuMnEPD exhibited the highest level of Cr evaporation of all the coated materials. Cr diffusion into the $(Cu,Mn)_3O_4$ spinel at temperatures >750 °C has been widely reported in the literature [51,52,67]. In addition, exposure to a higher pre-oxidation temperature (850 °C) for 100 h might have increased the Cr diffusion to the $(Cu,Mn)_3O_4$ spinel. Such diffusion was already observed in the as-received coupons shown in Fig. 2e. Nevertheless, the $(Cu,Mn)_3O_4$ spinel (225 S cm^{-1}) has been extensively researched for coating materials in SOFCs due to its high conductivity compared to the $(Co,Mn)_3O_4$ spinel (6.7–60.0 S cm^{-1}) [15] and lower cost. Moreover, the $(Cu,Mn)_3O_4$ spinel does not show Cr diffusion into the spinel at lower temperatures [18], making it ideal for use at lower temperatures.

3.5. Area-specific resistance

Fig. 8 shows the ex-situ-measured ASR values for the uncoated and coated steels exposed for 3000 h in air with 3% H_2O at 800 °C. The ASR values of the samples plotted in Fig. 8 are half the measured values, i.e., for one face of the exposed coupon. The uncoated coupons showed the highest ASR values after 3000 h of exposure. This matches well with the thick chromia-rich scale observed in Fig. 5, which is composed of a $(Cr,Mn)_3O_4$ spinel and Cr_2O_3. Although the $(Cr,Mn)_3O_4$ spinel (0.02 S cm^{-1}) [15] is more-conductive than the Cr_2O_3 (0.008 S cm^{-1}) [68] at 800 °C and the $(Cr,Mn)_3O_4$ layer contributes with less than 20% of the total scale, the ASR is expected to be dominated by Cr_2O_3. On the other hand, the conductivity of the $(Cr,Mn)_3O_4$ spinel is significantly lower than that of the $(Co,Mn)_3O_4$ spinel (6.7–60.0 S cm^{-1}) [15] at 800 °C.

The coated steels showed lower ASR values than the uncoated Crofer 22 APU after 3000 h of exposure. This shows the beneficial effects of the coatings. All of the coated steels, with the exception of MCOEPD, showed ASR values in the range of 15–25 mΩ cm^2 after 3000 h, irrespective of coating thickness, composition and deposition method. This is in line with the earlier findings reported by Goebel et al. [69] showing that the conductivity of the coating does not determine the ASR, since the conductivity of Cr_2O_3 (0.008 S cm^{-1}) [68] is significantly lower than that of the $(Co,Mn)_3O_4$ spinel (6.7–60 S cm^{-1}) [15] at 800 °C. In support of this, the MCFAPS-coated steel with ~100 μm of coating oxide exhibited an ASR value similar to that for CeCoPVD-coated steel with ~1 μm of coating oxide. The pre-treated samples, MCFCuEPD, MCOGdIEPD and MCOCeUSC, which exhibited the lowest mass gains, had slightly lower ASR values compared to the other coated steels due to the presence of thinner chromia scale.

The MCOEPD-coated steel, despite having a similar chromia scale thickness as the MCOCeSP-, CeCoPVD-, and MCFAPS-coated steels, exhibited a substantially higher ASR value than any of the other samples. The high ASR value of MCOEPD might be due to poor contact between the platinum electrodes/platinum paste and the coating. This notion is supported by the results of an additional ASR measurement that was performed with an as-received coating with a very thin chromia scale (pre-oxidised at 800 °C for 5 h), for which an ASR value of 30 mΩ cm^{-2} was recorded.

4. Conclusions

The present study compares uncoated Crofer 22 APU to eight different coatings on Crofer 22 APU in air + 3% H_2O for up to 3000 h at 800 °C. The coatings were deposited using various techniques, such as APS, EPD, PVD, SP and USC. Most of the coatings were based on $(Co,Mn)_3O_4$, with the exception of one coating based on $(Cu,Mn)_3O_4$. The oxidation kinetics, chromium evaporation rate, and ASR of the coated steels were compared with uncoated Crofer 22 APU, to determine the effectiveness of the coatings. The as-received coatings differed in

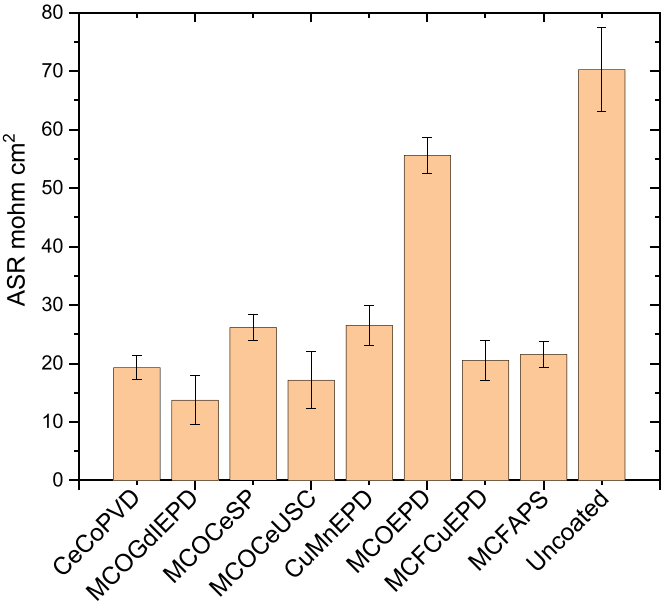

Fig. 8. The ex-situ area-specific resistances of the uncoated and coated Crofer 22 APU samples exposed for 3000 h in air +3% H_2O at 800 °C, measured using a 4-point mode with a current of 100 mA cm^{-2}.

thickness, ranging from 0.6 μm to 100 μm. After coating deposition, some of the coated steels were pre-treated in reducing and oxidising atmospheres.

All of the coated Crofer 22 APU samples showed lower chromium evaporation rates than the uncoated Crofer 22 APU samples. The (Co,Mn)$_3$O$_4$ based coatings reduced the chromium evaporation rate 50–100-fold, while the (Cu,Mn)$_3$O$_4$-based coating reduced the chromium evaporation rate 3–5-fold. The oxidation kinetics of the coated steels were lower than that of the uncoated Crofer 22 APU. The (Co,Mn)$_3$O$_4$-based coated steels with pre-treatment at temperatures >900 °C showed significantly lower oxidation kinetics compared to the other coated materials. An intermediate Cr enriched layer between the coating and chromia scale was found in such coated steels. Compared to the uncoated steel, all the coated samples showed lower ASR values after 3000 h of exposure, irrespective of coating thickness, composition or deposition method and the presence of an intermediate layer.

CRediT authorship contribution statement

Mareddy Jayanth Reddy: Conceptualization, Investigation, Writing – original draft, Writing – review & editing. **Bartosz Kamecki:** Resources, Writing – review & editing. **Belma Talic:** Resources, Writing – review & editing. **Elisa Zanchi:** Resources, Writing – review & editing. **Federico Smeacetto:** Resources, Writing – review & editing. **John S. Hardy:** Resources, Writing – review & editing. **Jung Pyung Choi:** Resources, Writing – review & editing. **Łukasz Mazur:** Resources, Writing – review & editing. **Robert Vaßen:** Resources, Writing – review & editing. **Soumendra N. Basu:** Resources, Writing – review & editing. **Tomasz Brylewski:** Resources, Writing – review & editing. **Jan-Erik Svensson:** Writing – review & editing, Supervision, Funding acquisition. **Jan Froitzheim:** Conceptualization, Writing – review & editing, Funding acquisition, Supervision, Project administration.

Declaration of competing interest

The authors declare that they have no known competing financial interests or personal relationships that could have appeared to influence the work reported in this paper.

Data availability

Data will be made available on request.

Acknowledgements

Sebastian Molin (Gdańsk University of Technology) and Srikanth Gopalan (Boston University) helped to facilitate this work. Furthermore, this work was supported by the strategic innovation program Metalliska Material (Vinnova grant 2021–01003) a joint program of VINNOVA, Formas and the Swedish Energy. This work was conducted at the Swedish High Temperature Corrosion Centre (HTC) at Chalmers University of Technology. This work was performed in part at the Chalmers Material Analysis Laboratory (CMAL).

References

[1] A. Buonomano, F. Calise, M.D. d'Accadia, A. Palombo, M. Vicidomini, Hybrid solid oxide fuel cells-gas turbine systems for combined heat and power: a review, Appl. Energy 156 (2015) 32–85.
[2] A. Choudhury, H. Chandra, A. Arora, Application of solid oxide fuel cell technology for power generation - a review, Renew. Sustain. Energy Rev. 20 (2013) 430–442.
[3] C. Goebel, et al., Long-term (4 year) degradation behavior of coated stainless steel 441 used for solid oxide fuel cell interconnect applications, J. Power Sources 449 (2020).
[4] M. Bianco, J.P. Ouweltjes, J. Van herle, Degradation analysis of commercial interconnect materials for solid oxide fuel cells in stacks operated up to 18000 hours, Int. J. Hydrogen Energy 44 (2019) 31406–31422.
[5] C.M. Harrison, P.R. Slater, R. Steinberger-Wilckens, A review of Solid Oxide Fuel Cell cathode materials with respect to their resistance to the effects of chromium poisoning, Solid State Ionics 354 (2020), 115410.
[6] S.P. Jiang, X. Chen, Chromium deposition and poisoning of cathodes of solid oxide fuel cells - a review, Int. J. Hydrogen Energy 39 (2014) 505–531.
[7] T. Brylewski, et al., Influence of Gd deposition on the oxidation behavior and electrical properties of a layered system consisting of Crofer 22 APU and MnCo2O4 spinel, Int. J. Hydrogen Energy 46 (2021) 6775–6791.
[8] J.G. Grolig, J. Froitzheim, J.E. Svensson, Coated stainless steel 441 as interconnect material for solid oxide fuel cells: oxidation performance and chromium evaporation, J. Power Sources 248 (2014) 1007–1013.
[9] S. Canovic, et al., Oxidation of Co- and Ce-nanocoated FeCr steels: a microstructural investigation, Surf. Coating. Technol. 215 (2013) 62–74.
[10] W. Qu, L. Jian, D.G. Ivey, J.M. Hill, Yttrium, cobalt and yttrium/cobalt oxide coatings on ferritic stainless steels for SOFC interconnects, J. Power Sources 157 (2006) 335–350.
[11] W.Z. Zhu, S.C. Deevi, Development of interconnect materials for solid oxide fuel cells, Mater. Sci. Eng., A 348 (2003) 227–243.
[12] N. Shaigan, W. Qu, D.G. Ivey, W. Chen, A review of recent progress in coatings, surface modifications and alloy developments for solid oxide fuel cell ferritic stainless steel interconnects, J. Power Sources 195 (2010) 1529–1542.
[13] M.J. Reddy, J.-E. Svensson, J. Froitzheim, Reevaluating the Cr evaporation characteristics of Ce/Co coatings for interconnect applications, ECS Trans. 103 (2021) 1899–1905.
[14] M.J. Reddy, T.E. Chausson, J.E. Svensson, J. Froitzheim, 11–23% Cr steels for solid oxide fuel cell interconnect applications at 800 °C – how the coating determines oxidation kinetics, Int. J. Hydrogen Energy (2023), https://doi.org/10.1016/j.ijhydene.2022.11.326.
[15] A. Petric, H. Ling, Electrical conductivity and thermal expansion of spinels at elevated temperatures, J. Am. Ceram. Soc. 90 (2007) 1515–1520.
[16] J.G. Grolig, P. Alnegren, J. Froitzheim, J.E. Svensson, Copper iron conversion coating for solid oxide fuel cell interconnects, J. Power Sources 297 (2015) 534–539.
[17] H. Falk-Windisch, J. Claquesin, M. Sattari, J.E. Svensson, J. Froitzheim, Co- and Ce/Co-coated ferritic stainless steel as interconnect material for intermediate temperature solid oxide fuel cells, J. Power Sources 343 (2017) 1–10.
[18] M. Tomas, V. Asokan, J. Puranen, J.E. Svensson, J. Froitzheim, Efficiencies of cobalt- and copper-based coatings applied by different deposition processes for applications in intermediate-temperature solid oxide fuel cells, Int. J. Hydrogen Energy 47 (2022) 32628–32640.
[19] Q. Zhao, S. Geng, G. Chen, F. Wang, Application of sputtered NiFe2 alloy coating for SOFC interconnect steel, J. Alloys Compd. 769 (2018) 120–129.
[20] B. Hua, et al., A promising NiCo2O4 protective coating for metallic interconnects of solid oxide fuel cells, J. Power Sources 195 (2010) 7375–7379.
[21] P. Paknahad, M. Askari, M. Ghorbanzadeh, Application of sol–gel technique to synthesis of copper–cobalt spinel on the ferritic stainless steel used for solid oxide fuel cell interconnects, J. Power Sources 266 (2014) 79–87.
[22] A.M. Dayaghi, M. Askari, P. Gannon, Pre-treatment and oxidation behavior of sol–gel Co coating on 430 steel in 750 °C air with thermal cycling, Surf. Coating. Technol. 206 (2012) 3495–3500.
[23] G. Jalilvand, M.A. Faghihi-Sani, Fe doped Ni–Co spinel protective coating on ferritic stainless steel for SOFC interconnect application, Int. J. Hydrogen Energy 38 (2013) 12007–12014.
[24] E. Zanchi, et al., Electrophoretic co-deposition of Fe2O3 and Mn1,5Co1,5O4: processing and oxidation performance of Fe-doped Mn-Co coatings for solid oxide cell interconnects, J. Eur. Ceram. Soc. 39 (2019) 3768–3777.
[25] A.G. Sabato, et al., Mn-Co spinel coatings on Crofer 22 APU by electrophoretic deposition: up scaling, performance in SOFC stack at 850 °C and compositional modifications, J. Eur. Ceram. Soc. 41 (2021) 4496–4504.
[26] Z. Sun, et al., CuMn1.8O4 protective coatings on metallic interconnects for prevention of Cr-poisoning in solid oxide fuel cells, J. Power Sources 378 (2018) 125–133.
[27] E. Zanchi, et al., Recent advances on spinel-based protective coatings for solid oxide cell metallic interconnects produced by electrophoretic deposition, Mater. Lett. 286 (2021), 129229.
[28] R. Pinto, M.J. Carmezim, M.F. Montemor, Electrodeposition and isothermal aging of Co and Mn layers on stainless steel for interconnectors: initial stages of spinel phase formation, J. Power Sources 255 (2014) 251–259.
[29] Q.X. Fu, D. Sebold, F. Tietz, H.P. Buchkremer, Electrodeposited cobalt coating on Crofer22APU steels for interconnect applications in solid oxide fuel cells, Solid State Ionics 192 (2011) 376–382.
[30] R.K. Lenka, P.K. Patro, J. Sharma, T. Mahata, P.K. Sinha, Evaluation of $La_{0.75}Sr_{0.25}Cr_{0.5}Mn_{0.5}O_3$ protective coating on ferritic stainless steel interconnect for SOFC application, Int. J. Hydrogen Energy 41 (2016) 20365–20372.
[31] S.-I. Lee, et al., Highly dense Mn-Co spinel coating for protection of metallic interconnect of solid oxide fuel cells, J. Electrochem. Soc. 161 (2014) F1389–F1394.
[32] B. Talic, P.V. Hendriksen, K. Wiik, H.L. Lein, Thermal expansion and electrical conductivity of Fe and Cu doped MnCo2O4 spinel, Solid State Ionics 326 (2018) 90–99.
[33] Y. Xie, W. Qu, B. Yao, N. Shaigan, L. Rose, Dense protective coatings for SOFC interconnect deposited by spray pyrolysis, ECS Trans. 26 (2010) 357–362.
[34] S. Pandiyan, M. Bianco, A. El-Kharouf, R.I. Tomov, R. Steinberger-Wilckens, Evaluation of inkjet-printed spinel coatings on standard and surface nitrided ferritic stainless steels for interconnect application in solid oxide fuel cell devices, Ceram. Int. 48 (2022) 20456–20466.

[35] G.D. Han, et al., Fabrication of lanthanum strontium cobalt ferrite (LSCF) cathodes for high performance solid oxide fuel cells using a low price commercial inkjet printer, J. Power Sources 306 (2016) 503–509.
[36] L.C. Ajitdoss, et al., Mn1.5Co1.5O4 protective coating on Crofer22APU produced by thermal co-evaporation for SOFCs, Mater. Lett. 95 (2013) 82–85.
[37] S. Molin, et al., Microstructural and electrical characterization of Mn-Co spinel protective coatings for solid oxide cell interconnects, J. Eur. Ceram. Soc. 37 (2017) 4781–4791.
[38] J. Puranen, et al., Influence of powder composition and manufacturing method on electrical and chromium barrier properties of atmospheric plasma sprayed spinel coatings prepared from $MnCo_2O_4$ and Mn_2CoO_4 + Co powders on Crofer 22 AP, Int. J. Hydrogen Energy 39 (2014) 17246–17257.
[39] R. Spotorno, et al., Microstructural and electrical characterization of plasma sprayed Cu-Mn oxide spinels as coating on metallic interconnects for stacking solid oxide fuel cells, Fuel Cell. 15 (2015) 728–734.
[40] N. Grünwald, et al., Microstructure and phase evolution of atmospheric plasma sprayed Mn-Co-Fe oxide protection layers for solid oxide fuel cells, J. Eur. Ceram. Soc. 39 (2019) 449–460.
[41] R. Vaßen, et al., Aging of atmospherically plasma sprayed chromium evaporation barriers, Surf. Coating. Technol. 291 (2016) 115–122.
[42] N. Grünwald, et al., In situ investigation of atmospheric plasma-sprayed Mn–Co–Fe–O by synchrotron X-ray nano-tomography, J. Mater. Sci. 55 (2020) 12725–12736.
[43] B. Talic, S. Molin, K. Wiik, P.V. Hendriksen, H.L. Lein, Comparison of iron and copper doped manganese cobalt spinel oxides as protective coatings for solid oxide fuel cell interconnects, J. Power Sources 372 (2017) 145–156.
[44] Q. Zhao, S. Geng, G. Chen, F. Wang, Comparison of electroplating and sputtering Ni for Ni/$NiFe_2$ dual layer coating on ferritic stainless steel interconnect, Corrosion Sci. 192 (2021).
[45] M. Bianco, et al., In-situ experimental benchmarking of solid oxide fuel cell metal interconnect solutions, J. Power Sources 461 (2020), 228163.
[46] M. Bianco, et al., Ex-situ experimental benchmarking of solid oxide fuel cell metal interconnects, J. Power Sources 437 (2019), 226900.
[47] J. Froitzheim, H. Ravash, E. Larsson, L.G. Johansson, J.E. Svensson, Investigation of chromium volatilization from FeCr interconnects by a denuder technique, J. Electrochem. Soc. 157 (2010) B1295.
[48] J.G. Grolig, J. Froitzheim, J.E. Svensson, Coated stainless steel 441 as interconnect material for solid oxide fuel cells: evolution of electrical properties, J. Power Sources 284 (2015) 321–327.
[49] B. Talic, et al., Effect of coating density on oxidation resistance and Cr vaporization from solid oxide fuel cell interconnects, J. Power Sources 354 (2017) 57–67.
[50] B. Kamecki, et al., Deposition and electrical and structural properties of La0.6Sr0.4CoO3 thin films for application in high-temperature electrochemical cells, J. Electron. Mater. (2019) 5428–5441, 2019 489 48.
[51] M. Tomas, C. Goebel, J.-E. Svensson, J. Froitzheim, Cu-based coatings for IT-SOFC applications, ECS Trans. 91 (2019) 2291–2298.
[52] Y.A. Farzin, I. Ritucci, B. Talic, R. Kiebach, H.L. Frandsen, Fracture toughness of reactive bonded Co–Mn and Cu–Mn contact layers after long-term aging, Ceram. Int. 48 (2022) 20699–20711.
[53] H. Falk-Windisch, J.E. Svensson, J. Froitzheim, The effect of temperature on chromium vaporization and oxide scale growth on interconnect steels for Solid Oxide Fuel Cells, J. Power Sources 287 (2015) 25–35.
[54] N. Grünwald, D. Sebold, Y.J. Sohn, N.H. Menzler, R. Vaßen, Self-healing atmospheric plasma sprayed Mn1.0Co1.9Fe0.1O4 protective interconnector coatings for solid oxide fuel cells, J. Power Sources 363 (2017) 185–192.
[55] A.C.S. Sabioni, et al., Study of ion diffusion in oxidation films grown on a model Fe–15%Cr alloy, Solid State Ionics 276 (2015) 1–8.
[56] M.J. Reddy, Metallic Materials in Solid Oxide Fuel Cells: Oxidation and Chromium Evaporation Properties, Chalmers University of Technology, 2021.
[57] Z. Yang, et al., Structure and conductivity of thermally grown scales on ferritic Fe-Cr-Mn steel for SOFC interconnect applications, J. Electrochem. Soc. 151 (2004).
[58] M. Stanislowski, E. Wessel, K. Hilpert, T. Markus, L. Singheiser, Chromium vaporization from high-temperature alloys, J. Electrochem. Soc. 154 (2007) A295.
[59] J. Froitzheim, et al., Long term study of Cr evaporation and high temperature corrosion behaviour of Co coated ferritic steel for solid oxide fuel cell interconnects, J. Power Sources 220 (2012) 217–227.
[60] N.J. Magdefrau, L. Chen, E.Y. Sun, J. Yamanis, M. Aindow, Formation of spinel reaction layers in manganese cobaltite-coated Crofer22 APU for solid oxide fuel cell interconnects, J. Power Sources 227 (2013) 318–326.
[61] E. Zanchi, et al., Iron doped manganese cobaltite spinel coatings produced by electrophoretic co-deposition on interconnects for solid oxide cells: microstructural and electrical characterization, J. Power Sources 455 (2020).
[62] S. Fontana, et al., Metallic interconnects for SOFC: characterisation of corrosion resistance and conductivity evaluation at operating temperature of differently coated alloys, J. Power Sources 171 (2007) 652–662.
[63] Y. Yan, R. Bateni, J. Harris, O. Kesler, Fabrication of reactive element oxide coatings on porous ferritic stainless steel for use in metal-supported solid oxide fuel cells, Surf. Coating. Technol. 272 (2015) 415–427.
[64] S. Fontana, M. Vuksa, S. Chevalier, G. Caboche, P. Piccardo, On the effect of surface treatment to improve oxidation resistance and conductivity of metallic interconnects for SOFC in operating conditions, Mater. Sci. Forum 595–598 (2008) 753–762.
[65] M. Sattari, R. Sachitanand, J. Froitzheim, J.E. Svensson, T. Jonsson, The Effect of Ce on the High Temperature Oxidation Properties of a Fe–22%Cr Steel: Microstructural Investigation and EELS Analysis, vol. 32, 2015, pp. 118–122.
[66] J.G. Grolig, J. Froitzheim, J.E. Svensson, Effect of cerium on the electrical properties of a cobalt conversion coating for solid oxide fuel cell interconnects - a study using impedance spectroscopy, Electrochim. Acta 184 (2015) 301–307.
[67] Z. Zhu, et al., Comparison of Cu–Mn and Mn–Co spinel coatings for solid oxide fuel cell interconnects, Int. J. Hydrogen Energy (2022), https://doi.org/10.1016/J.IJHYDENE.2022.08.239.
[68] J.-H. Park, K. Natesan, Electronic transport in thermally grown Cr2O3, Oxid. Metals (1990) 31–54, 1990 331 33.
[69] C. Goebel, A.G. Fefekos, J.E. Svensson, J. Froitzheim, Does the conductivity of interconnect coatings matter for solid oxide fuel cell applications? J. Power Sources 383 (2018) 110–114.
[70] C. Goebel, et al., Long term (4 Years) performance of Co/Ce coated 441 for SOFC interconnect applications, ECS Trans. 78 (2017) 1675–1679.
[71] Ł. Mazur, et al., Effectiveness of a dual surface modification of metallic interconnects for application in energy conversion devices, Int. J. Hydrogen Energy 47 (2022) 6295–6311.
[72] B. Kamecki, et al., Low temperature deposition of dense MnCo2O4 protective coatings for steel interconnects of solid oxide cells, J. Eur. Ceram. Soc. 38 (2018) 4576–4579.
[73] D. Szymczewska, S. Molin, P.V. Hendriksen, P. Jasiński, Microstructure and electrical properties of Fe,Cu substituted (Co,Mn)3O4 thin films, Cryst 7 (2017), 185 7, 185 (2017).
[74] J.P. Choi, K. Scott Weil, Y. Matt Chou, J.W. Stevenson, Z. Gary Yang, Development of MnCoO coating with new aluminizing process for planar SOFC stacks, Int. J. Hydrogen Energy 36 (2011) 4549–4556.
[75] R. Wang, et al., Ferritic stainless steel interconnects for protonic ceramic electrochemical cell stacks: oxidation behavior and protective coatings, Int. J. Hydrogen Energy 44 (2019) 25297–25309.
[76] W. Huang, S. Gopalan, U.B. Pal, S.N. Basu, Evaluation of electrophoretically deposited CuMn[sub 1.8]O[sub 4] spinel coatings on crofer 22 APU for solid oxide fuel cell interconnects, J. Electrochem. Soc. 155 (2008) B1161.
[77] B. Talic, V. Venkatachalam, P.V. Hendriksen, R. Kiebach, Comparison of MnCo2O4 coated Crofer 22 H, 441, 430 as interconnects for intermediate-temperature solid oxide fuel cell stacks, J. Alloys Compd. 821 (2020), 153229.
[78] E. Zanchi, et al., Electrophoretic co-deposition of Mn1.5Co1.5O4, Fe2O3 and CuO: unravelling the effect of simultaneous addition of Cu and Fe on the microstructural, thermo-mechanical and corrosion properties of in-situ modified spinel coatings for solid oxide cell interconnects, J. Eur. Ceram. Soc. 42 (2022) 3271–3281.
[79] M. Stanislowski, et al., Reduction of chromium vaporization from SOFC interconnectors by highly effective coatings, J. Power Sources 164 (2007) 578–589.
[80] E. Dogdibegovic, et al., Performance of stainless steel interconnects with (Mn,Co)3O4-Based coating for solid oxide electrolysis, Int. J. Hydrogen Energy 47 (2022) 24279–24286.
[81] M. Casteel, D. Lewis, P. Willson, M. Alinger, Ionic Conductivity Method for measuring vaporized chromium species from solid oxide fuel cell interconnects, Int. J. Hydrogen Energy 37 (2012) 6818–6829.
[82] R. Trebbels, T. Markus, L. Singheiser, Reduction of chromium evaporation with manganese-based coatings, ECS Trans. 25 (2009) 1417–1422.
[83] W. Wongpromrat, et al., Reduction of chromium volatilisation from stainless steel interconnector of solid oxide electrochemical devices by controlled preoxidation, Corrosion Sci. 106 (2016) 172–178.
[84] T. Thublaor, S. Chandra-ambhorn, High temperature oxidation and chromium volatilisation of AISI 430 stainless steel coated by Mn-Co and Mn-Co-Cu oxides for SOFC interconnect application, Corrosion Sci. 174 (2020), 108802.
[85] H. Kurokawa, C.P. Jacobson, L.C. DeJonghe, S.J. Visco, Chromium vaporization of bare and of coated iron-chromium alloys at 1073 K, Solid State Ionics 178 (2007) 287–296.
[86] C. Collins, et al., Chromium volatility of coated and uncoated steel interconnects for SOFCs, Surf. Coating. Technol. 201 (2006) 4467–4470.
[87] H. Chen, et al., Thermal stability and oxidation resistance of TiCrAlYO coatings on SS430 for solid oxide fuel cell interconnect applications, Surf. Coating. Technol. 202 (2008) 4820–4824.